Article

A Combined Multiple Factor Degradation Model and Online Verification for Electric Vehicle Batteries

Yuan Chen [1], **Yigang He [1,*]**, **Zhong Li [2] and Liping Chen [1]**

[1]   School of Electrical Engineering and Automation, Hefei University of Technology, Hefei 230009, China;
     2014010034@mail.hfut.edu.cn (Y.C.); lip_chen@hfut.edu.cn (L.C.)
[2]   Jianghuai Automobile Co. Ltd, Hefei 230092, China; jac_lizhong@163.com
[*]   Correspondence: yghe@hfut.edu.cn

check for
updates

Abstract: Battery state of health (SOH) is related to the reduction of total capacity due to complicated aging mechanisms known as calendar aging and cycle aging. In this study, a combined multiple factor degradation model was established to predict total capacity fade considering both calendar aging and cycle aging. Multiple factors including temperature, state of charge (SOC), and depth of discharge (DOD) were introduced into the general empirical model to predict capacity fade for electric vehicle batteries. Experiments were carried out under different aging conditions. By fitting the data between multiple factors and model parameters, battery degradation equations related to temperature, SOC, and DOD could be formulated. The combined multiple factor model could be formed based on the battery degradation equations. An online state of health estimation based on the multiple factor model was proposed to verify the correctness of the model. Predictions were in good agreement with experimental data for over 270 days, as the margin of error between the prediction data and the experimental data never exceeded 1%.

Keywords: combined multiple factor degradation model; calendar aging; cycle aging; online state-of-health prediction

1. Introduction

As the global population grows and the Earth's natural resources diminish, electric vehicles have been rapidly developed in recent years. When used in electric vehicles, lithium-ion batteries possess advantages, such as high energy density, long lifespans, no memory effect, environmental benignity, good stability, and affordability, when compared to other battery types, such as lead-acid batteries. As such, they are quickly becoming the first choice of battery type for electric vehicles.

The state of health (SOH) of batteries can be estimated, which provides useful information for battery management systems (BMS). Accurate capacity degradation modeling plays a significant role in battery prognostics and health management (PHM), as state of charge (SOC) estimation is related to battery capacity. Capacity prediction is very important for reliable operation and reduced maintenance costs of the battery management system [1].

Both model-based and data-based methods can be used to predict capacity fade. The data-based methods include fuzzy logic, artificial neural networks (ANN) [2,3], support-vector machines (SVM) [4], particle filters (PF) [5], unscented Kalman filters (UKF) [6], data-driven methods based on the Wiener process [7], and based on an autoregressive model [8]. The data-based methods for making SOH predictions are more complex as they require large amounts of data. Therefore, these methods are more suitable for making remaining useful life (RUL) predictions than online estimations.

Model-based methods capture the long-term dependencies of battery degradation based on mathematical aging models. The aging models can be divided into three categories: empirical models [9–

11], mechanical degradation models [12,13], and equivalent circuit models [14,15]. An empirical model can be obtained through the historical data mining of accelerated aging experiments. It is most commonly used in SOH predictions due to its mathematical simplicity, wide range of validity, and good adaptability. Examples of empirical models include the NREL Model [16], the Wang Model [17], and the MOBICUS Model [18]. Empirical models take into consideration the influence of factors such as temperature, SOC, depth of discharge (DOD), and discharge rate [19,20], but the quantitative analysis of these factors is still limited [21–26].

There are two different battery degradation scenarios of which to be mindful. One is calendar aging, which concerns the deterioration of battery characteristics when the battery is at storage. It is related to temperature and SOC. The other is cycle aging, which concerns the deterioration of battery characteristics with continuous use. It is related to temperature, discharge rate, and DOD [9].

Grolleau et al. proposed a simple modeling approach under time-dependent storage conditions (SOC and temperature) for making calendar aging predictions [18]. Experiments show that the deviation of predicted capacity based on that proposed model never exceeded 3% over 400 days and 5% over 625 days, but it is worth noting that Grolleau et al. used a calendar aging model that did not consider cycle aging. Cui et al. developed a multi-stress factor model that accounted for factors such as temperature, discharge rate, taper voltage, and depth of discharge for making battery cycle life predictions [21]. The practical applicability of this multi-stress factor model was proven by experimental data, but as the model did not consider calendar life predictions, it is therefore only suitable for making offline batter $Q_{calendar} = 1 - A \times \exp(\frac{-E_a}{RT}) \times t^{0.5}$ y cycle life predictions. In practical automotive applications, calendar aging and cycle aging occur simultaneously. Therefore, it is important that studies of battery SOH predictions account for both calendar and cycle life under actual driving conditions.

This paper focuses on the impact of stress factors on battery calendar and cycle life. The effects of four factors—temperature, discharge rate, SOC, and DOD—were analyzed. Battery degradation equations related to temperature, SOC, and DOD were formulated. A combined multiple factor model was also formed based on these battery degradation equations, considering both calendar aging and cycle aging. An online SOH prediction method on the basis of the proposed model was conducted under test conditions. The practical applicability of the model was validated by experimental data.

2. Degradation Model

An empirical calendar degradation model was set up as Equation (1) and is shown referring to the Arrhenius equation [16].

$$Q_{calendar} = 1 - A \times \exp(\frac{-E_a}{RT}) \times t^{0.5} \tag{1}$$

where $Q_{calendar}$ is the relative capacity after calendar degradation (Ah), A is the pre-exponential factor, T is temperature of cell (K), E_a is activation energy (Jmol^{-1}), R is gas constant (8.314 J/mol/K), 0.5 of $t^{0.5}$ is most widely accepted as a time trend enhancement factor due to the Solid Electrolyte Interface (SEI) layer growth [13], and t is storage time.

The cycle degradation model is built similarly to the calendar one according to battery degradation mechanisms [9,16,17].

$$Q_{cycle} = 1 - B \times \exp(\frac{-E_a}{RT}) \times N^{0.5} \tag{2}$$

where Q_{cycle} is the relative capacity of cycle degradation (Ah), B is the pre-exponential factor, and N is the cycle number.

The parameters of the calendar and cycle degradation model were obtained by recursive least squares (RLS).

3. Experiment and Discussion

The batteries used were INR18650-33G batteries made by Samsung. Battery parameters were as shown in Table 1. The experimental data were collected via the battery test platform. The main test instruments, as shown in Figure 1, were a charge and discharge test system for lithium batteries (Arbin BT2000) and a thermal chamber for environmental control (HL T402P made by Haoyuan Environmental Testing Equipment Co., Ltd in Qongqing).

Table 1. Battery parameters of INR18650-33G.

	Item	Value
INR18650-33G	Capacity	2.8 Ah
	Charging C-rate	0.15 C, 0.33 C, 0.5 C, 0.7 C, 1.0 C
	Discharging C-rate	0.33 C, 0.5 C, 1.0 C, 1.5 C, 2.0 C, 3.0 C, 4.0 C
	T range for storage	−40°–60°
	T range for charge	−10°–45°
	T range for discharge	−20°–60°
	Upper cutoff voltage	4.1 V
	Lower cutoff voltage	2.5 V
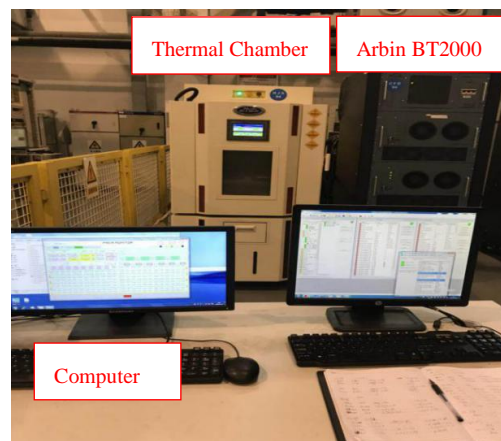
Figure 1. Battery test platform.

Before the experiments, the static capacity test was conducted at 25°. It provided a reference for measuring the nominal capacity of a fresh cell. During the test, two cells were charged at 0.5 C in a constant-current constant-voltage mode to the upper cutoff voltage of − 4.1 V. The test would stop when the current was at 0.03 C (0.06 A). The cells were left to rest for one hour without load, in order for them to stabilize. They were then discharged at 0.5 C to the lower cutoff voltage of − 2.5 V. The cells were again left to rest for an hour without load to stabilize. This cycle was repeated twice, and the average capacity of the battery was taken as a reference.

The calendar and cycle aging experiments were conducted respectively under different conditions according to national standards of automotive applications (GBT 31484-2015).

3.1. Calendar Aging Experiments

Two parameters have been investigated in calendar aging experiments: temperature and SOC. Three groups of six 18,650 cells with a 2780 mAh nominal capacity were stored in thermal chambers at three temperatures (25°, 45°, 60°). Six cells were charged at six nominal states of charge: 20%, 40%, 50%, 60%, 80%, and 100%, respectively. The cells were stored for 270 days.

The calendar aging experiments were performed as follows:

1. The static capacity test was conducted as described in Section 3;
2. The cells were charged with 0.5 C in a constant-current mode at 25° to reach six nominal states of charge: 20%, 40%, 50%, 60%, 80%, and 100%;
3. The cells were stored at 25°, 45°, and 60° for 30 days;
4. The battery cells were calibrated after step 3;
5. Steps 2–4 were repeated to test multiple cells.

3.1.1. Capacity Fitted Curves

From the calendar aging experiments, a set of corresponding Q, T, and t can be obtained. The experimental data are substituted into the calendar degradation model, and model parameters obtained by the recursive least squares method are shown in Table 2.

Table 2. Calendar aging model parameters under different conditions.

Temperature	State of Charge (*SOC*)	*A*	*Ea/R*
25°	20%	73	3065
	40%	153	3064
	50%	162	3053
	60%	147	3067
	80%	129	3062
	100%	95	3047
45°	20%	76	3069
	40%	156	3066
	50%	158	3041
	60%	142	3043
	80%	135	3061
	100%	101	3058
60°	20%	69	3073
	40%	148	3059
	50%	150	3054
	60%	141	3047
	80%	125	3061
	100%	98	3055

The degradation model fitted with experimental data is shown in Figure 2. The lines are fitted curves and the triangles are the experimental data. Both the model-fitted data and experimental data agree well. At 60°, the error of capacity is slightly larger than other temperatures.

The battery degradation is mainly caused by the growth of the SEI film on the negative surface of the battery in the early stage of aging (10% before capacity decay). The SEI film is essentially a side reaction byproduct of the electrolyte and the embeddable lithium ion. Its growth rate depends on the decomposition rate of the electrolyte on the surface of the negative electrode. The decomposition belongs to a kind of chemical reaction. It is affected by temperature, anode potential, and concentration of related reactants (such as lithium ions). It can be seen from the calendar experiments that the temperature had a great influence on the battery capacity, and the storage SOC also had a certain degree of influence on it.
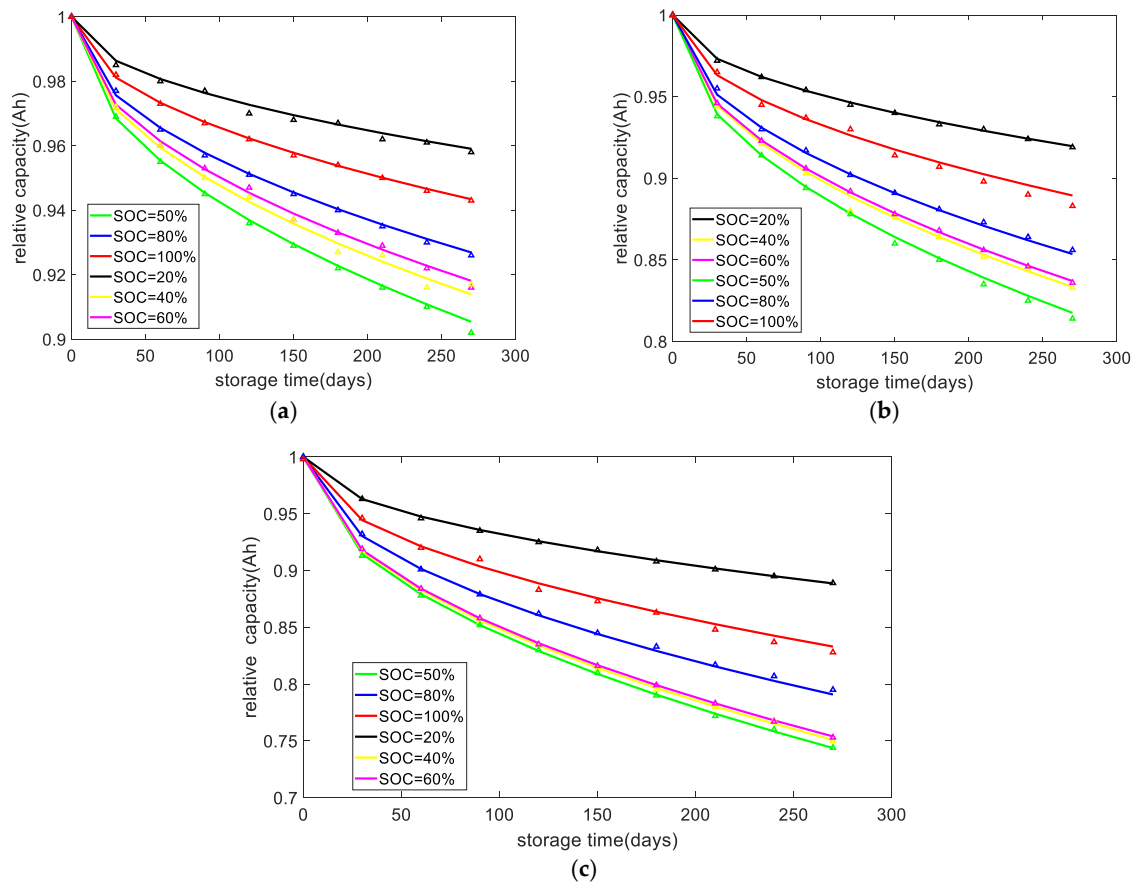
Figure 2. Capacity (experimental data and fit) under six storage SOCs (20%, 40%, 50%, 60%, 80%, and 100%) (**a**) at 25°, (**b**) at 45°, and (**c**) at 60°.

3.1.2. The Analysis of Factors

Due to the formula $\ln(A_0) = \ln(A) - \frac{E_a}{RT}$, the fitting results of $-\ln(A_0)$ and *1/T* are shown in Figure 3. On the plot, $-\ln(A)$ are the values of y-intercept and $\frac{E_a}{R}$ are the slopes. $\frac{E_a}{R}$ can be set to 3053, as the values under different working conditions are nearly identical, which means the values are independent of *SOC* and *T*. The relationships between $-\ln(A_0)$ and 1/*T* are linear, which means the pre-exponential factor *A* is insensitive to *T*. The values of *A* are determined only by *SOC*. The factors of temperature and storage *SOC* are irrelevant. A function can be introduced to describe the quantitative relationship of *A* with *SOC* change [9].
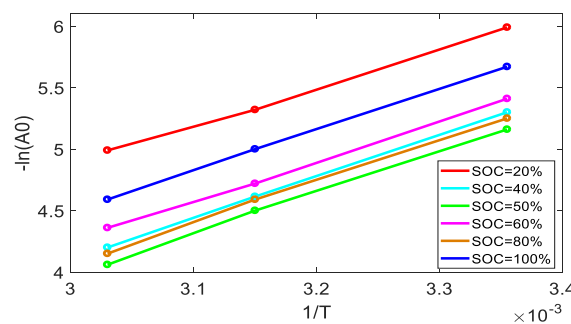
Figure 3. The fitting results of $-\ln(A_0)$ with 1/*T*.

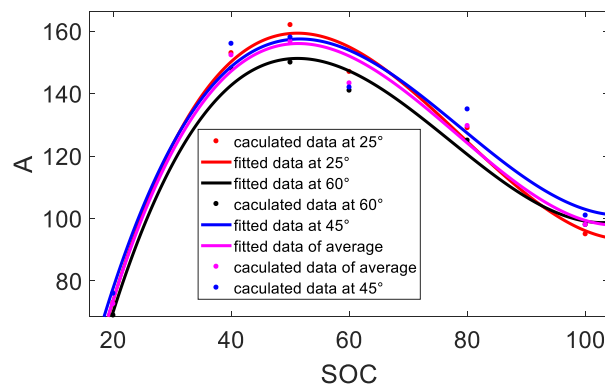The relationship between *SOC* and *A* is shown in Figure 4 using a curve fitting.

Figure 4. The relationship between SOC and A.

At 25°, 45° and 60°, the curves in Figure 4 change little. Taking average of the three curves, the pre-exponential factor related to *SOC* can be formulated as shown in Equation (3):

$$A = f(SOC) = 0.0007459 \times SOC^3 - 0.1751 \times SOC^2 + 12.08 \times SOC - 103.5. \tag{3}$$

The calendar capacity can be expressed as Equation (4) by substituting Equation (3) and $\frac{E_a}{R}$ into Equation (1).

$$Q_{calendar} = 1 - f(SOC) \times \exp(\frac{-3053}{T}) \times t^{0.5} \tag{4}$$

3.2. Cycle Aging Experiments

Three groups of experiments (temperature aging experiments, *DOD* aging experiments, and discharge rates aging experiments) were conducted within 900 cycles. Table 3 contains all of relevant parameters (discharge rates, *T*, *SoC*) proposed for each experiment. The capacity data were recorded every 30 cycles.

Table 3. All relevant parameters (discharge rates, *T*, *SoC*) for each experiment.

Name	Discharge Rates	*T*	Depth of Discharge (*DOD*)
Temperature aging experiments	0.5 C	10°, 25°, and 45°	60%
DOD aging experiments	0.5 C	25°	10%, 20%, 40%, 60%, 80%, 100%
Discharge rate aging experiments	0.5 C, 1 C, 3 C	25°	100%

The cycle temperature aging experiments were performed as follows:

1. The static capacity test was conducted as described in Section 3;
2. The cell was charged with 0.5 C in a constant-current constant-voltage mode until it was fully charged to cutoff voltage;
3. The test would stop when the current was at 0.03 C, then the cell would be left to rest with no load for one hour to stabilize;
4. The cell was discharged with 0.5 C in a constant-current mode at 25° to reach 40% SOC;
5. The cell was then left to rest with no load for 20 minutes;
6. Steps 2 and 3 were repeated to test 900 cycles.

The procedures of the cycle degradation experiments at 10° and 45° were the same as described above.

The *DOD* and discharge rate experiments were performed with similar steps to the temperature experiments.

3.2.1. Capacity Fitted Curves

Several sets of corresponding Q, T, and N can be obtained from cycle temperature experiments, *DOD* experiments, and discharge rate experiments, respectively. By the RLS method, model parameters at different temperatures, *DOD*, and discharge rate were calculated as shown in Tables 4–6.

Table 4. Cycle aging model parameters at different temperatures.

Temperature	B	Ea/R
10°	8691	4349
25°	8823	4352
45°	8785	4341

Table 5. Cycle aging model parameters at different *DODs*.

DOD	B	Ea/R
10%	8330	4356
20%	8440	4342
40%	8820	4347
60%	9860	4345
80%	12,330	4342
100%	13,990	4340

Table 6. Cycle aging model parameters at different discharge rates.

Discharge Rate	B	Ea/R
0.5 C	13,923	4349
1 C	10,630	4250
3 C	5285	3991

Capacity as a function of cycle number is plotted as shown in Figure 5. The lines are fitted curves, and the triangles are the experimental data. The prediction data are in good agreement with the experimental data, demonstrating the reliability and correctness of the cycle models.

Figure 5a displays capacity experimental data and fit at different temperatures. The results indicate that as temperature increases, the aging accelerates. The degradation at 45° for 900 cycles increased nearly 20% compared to that at 25°. Temperature is perhaps the most influential factor on the impact of capacity loss, as it affects the growth of SEI film.

Capacity at different DODs at 25° is plotted in Figure 5b. As the DOD of the battery increases, the rate of decay of the battery capacity gradually increases. The degradation under 100% DOD for 900 cycles increased about 10% compared to that under 10% DOD, illustrating that DOD is a less important factor in the model, especially at lower DODs (<60%).

The prediction model fitted with discharge rate experimental data is shown in Figure 5c. The degradation discharged at 3 C for 900 cycles increased about 4% compared to that at 0.5 C, indicating that the capacity loss is affected slightly by discharge rate. The SEI film is affected by the diversification of the concentration of reactants in lithium-ion batteries, which is caused by different DODs and discharge rates. The experimental results are consistent with the aging mechanism of the battery.
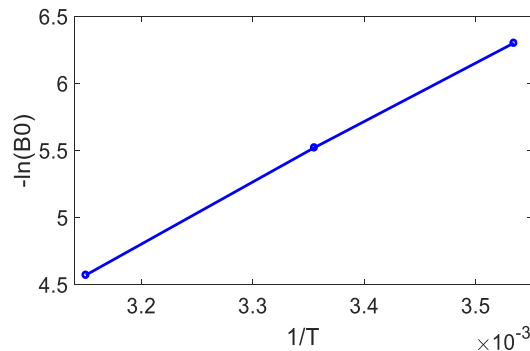
3.2.2. The Analysis of Factors

Due to the formula $\ln(B_0) = \ln(B) - \frac{E_a}{RT}$, the fitting results of $-\ln(B_0)$ and $1/T$ are shown in Figure 6.
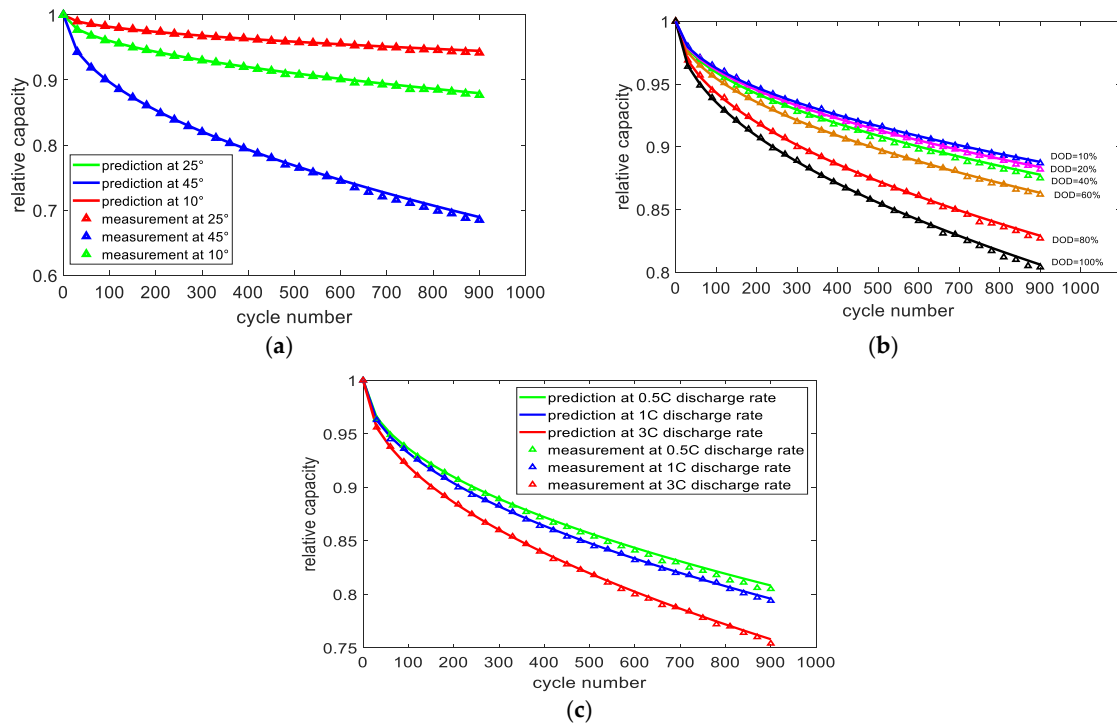
Figure 5. Capacity (experimental data and fit) (**a**) at different temperatures; (**b**) under different DODs; (**c**) at different discharge rates.


Figure 6. The fitting results of $-\ln(B_0)$ with $1/T$.

On the plot, $-\ln(B)$ are the values of y-intercept and $\frac{E_a}{R}$ are the slopes. The relationship between $-\ln(B_0)$ and *1/T* is linear, which means that the pre-exponential factor *B* is independent of *T*. $\frac{E_a}{R}$ values can be set to 4345 as the values under different *DODs* are nearly identical, as shown in Table 5. The pre-exponential factor *B* changes with *DOD*; the factor of temperature is irrelevant. A function using third-order polynomial can be introduced to describe the quantitative relationship of B with DOD change as shown in Equation (5) [9].

$$f(DOD) = -0.002315 \times DOD^3 + 1.071 \times DOD^2 - 27.49 \times DOD + 8473 \tag{5}$$

The fit between DOD and B can be seen in Figure 7.
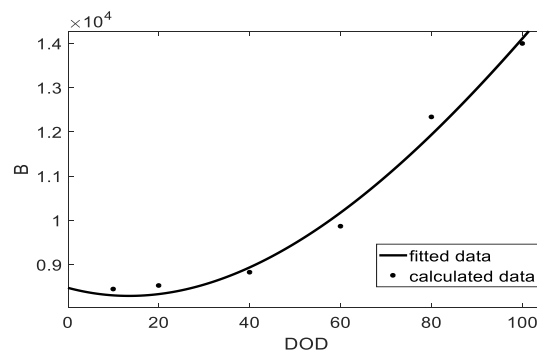
Figure 7. The relationship between DOD and B.

After a closer examination of the data in Table 4, discharge rate was chosen not to be considered, as it was found to be less important than cycle time.

The capacity can be expressed as Equation (6) by substituting Equation (5) and $\frac{E_a}{R}$ into Equation (2).

$$Q_{cycle} = 1 - f(DOD) \times \exp(\frac{-4345}{T}) \times N^{0.5}. \tag{6}$$

3.3. Online SOH Estimation Based on the Combined Multiple Factor Degradation Model and Verification

The degenerative effects of calendar aging and cyclic aging are considered additive, so a combined multiple factor degradation model can be built as Equation (7) by combining Equations (4) and (6).

$$\begin{cases} Q_{calendar} = 1 - f(SOC) \times \exp(\frac{-3053}{T}) \times t^{0.5} \\ Q_{cycle} = 1 - f(DOD) \times \exp(\frac{-4345}{T}) \times N^{0.5} \end{cases} \tag{7}$$

where t is the parking time (days) and N is the cycle number.

In electric vehicles, cycle conditions include driving and charging conditions, while calendar conditions include parking conditions. They both occur in electric vehicle working conditions. Based on the combined multiple factor degradation model, an online SOH estimation method can be used to verify the correctness of the model.

Experiments were conducted in the battery test platform. The battery was charged and discharged once per day, and the rest of the day was for parking. The test conditions of average temperature, storage SOC, and DOD are set every two months as in Table 7. It is a simplification and simulation of the actual working conditions of electric vehicles. The parking time can be measured in the platform shown in Table 7.

Table 7. Test conditions in the battery test platform.

Number of Days	Average Temperature	Storage SOC	DOD	Parking Time(day)
1–60	10°	100%	100%	20/24
61–120	20°	80%	80%	20.4/24
121–180	25°	60%	60%	20.2/24
181–240	35°	40%	40%	21.2/24
241–270	40°	20%	20%	21.6/24

The capacity degradation can be calculated by Equation (8).

$$\begin{cases} Q_{losscy}(i) = f(DOD_i) \times \exp(\frac{-4345}{T_i}) \times (n)^{0.5} \\ Q_{lossca}(i) = f(SOC_i) \times \exp(\frac{-3053}{T_i}) \times (k_i)^{0.5} \end{cases} \tag{8}$$

where Q_{losscy} is the capacity fade of cycle aging (Ah), Q_{lossca} is the capacity fade of calendar aging (Ah), i is the number of days, $i = 1:270$. SOC_i, DOD_i, T_i are the SOC, DOD, and temperature at the time of day i. n is the cycle number one day, and $n = 1$ as the battery is charged and discharged once a day. k_i is the parking time per day.

Q_{loss} can be calculated by Equation (9).

$$Q_{loss}(i) = \sum_{i=1}^{n} \left(Q_{losscy}(i) + Q_{lossca}(i) \right) \tag{9}$$

where Q_{loss} is the total capacity fade of the battery (Ah).

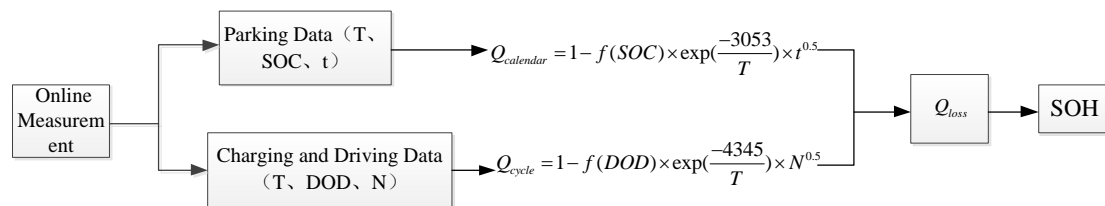The diagram of the online SOH estimation is shown in Figure 8.

Figure 8. The diagram of online state of health (SOH) estimation.

The actual capacity data are collected every 10 days in the platform. A comparison of predicted and measured data is shown as Figure 9a,b. It can be seen from Figure 9a,b that prediction data are in good agreement with the experimental results, to the point where the error never exceeded 1%.
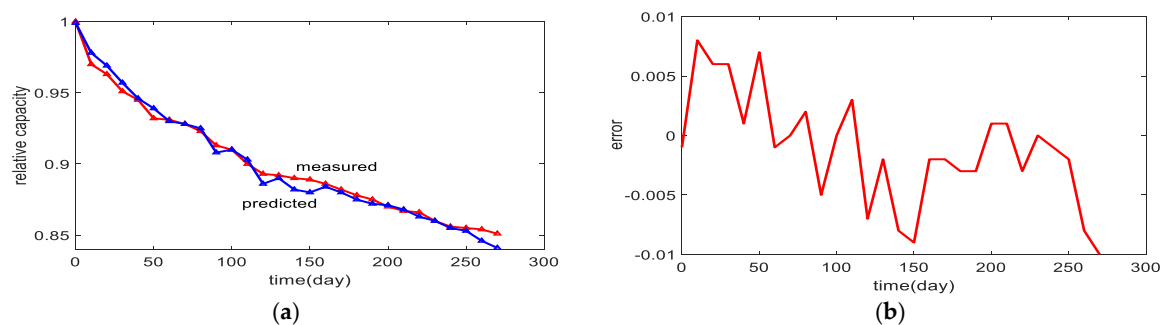

Figure 9. (**a**) Comparison between online prediction value and actual measurement value (**b**) capacity prediction error.

The results verify the correctness of the proposed model. When the battery operating conditions change, the model can reflect the degradation of the actual capacity very well. It can be used for an actual SOH prediction during the driving of an electric car.

4. Conclusions

In this paper, a combined multiple factor degradation model consisting of temperature, SOC, and DOD was established for calendar and cycle life predictions of electric vehicle batteries. Calendar and cycle aging experiments were conducted. Model pre-exponential factors, which reflect degradation reaction velocity depend only on SOC in calendar aging and on DOD in cycle aging. SOC and DOD as membership factors were introduced to calendar and cycle aging respectively to describe their impact on calendar and cycle degradation.

Based on the combined multiple factor degradation model, an online SOH estimation method was proposed to verify the correctness of the proposed model. The model reflected the degradation very well, with an error margin between prediction data and experimental data within 1%.

Conflicts of Interest: The authors declare no conflicts of interest.

Nomenclature

SOH	state of health
SOC	state of charge
DOD	depth of discharge
BMS	battery management system
PHM	prognostics and health management
ANN	artificial neural network
SVM	support vector machine
PF	particle filter
UKF	unscented Kalman filter
RUL	remaining useful life
A	coefficient of calendar degradation
T	temperature of cell
E_a	activation energy
R	gas constant (8.314 J/mol/K)
t	storage time
$Q_{calendar}$	the relative capacity of calendar degradation
SEI	Solid Electrolyte Interface
Q_{cycle}	the relative capacity of cycle degradation
B	coefficient of cycle degradation
N	cycle number
RLS	recursive least squares
Ah	Amp-hour
Q_{losscy}	the capacity fade of cycle aging
Q_{lossca}	the capacity fade of calendar aging
i	the number of the day
SOC_i	the SOC at the time of day i
DOD_i	the DOD at the time of day i
T_i	the temperature at the time of day i
k_i	the parking time of the day
Q_{loss}	the total capacity fade of the battery

References

1. Bevilacqua, M.; Braglia, M. The analytic hierarchy process applied to maintenance strategy selection. *Reliab. Eng. Syst. Saf.* **2000**, *70*, 71–83. [CrossRef]
2. Andre, D.; Nuhic, A.; Soczka-Guth, T.; Sauer, D.U. Comparative study of a structured neural network and an extended Kalman filter for state of health determination of lithium-ion batteries in hybrid electric vehicles. *Eng. Appl. Artif. Intell.* **2013**, *26*, 951–961. [CrossRef]
3. You, G.W.; Park, S.; Oh, D. Diagnosis of electric vehicle batteries using recurrent neural networks. *IEEE Trans. Ind. Electron.* **2017**, *64*, 4885–4893. [CrossRef]
4. Dong, H.; Jin, X.; Lou, Y.; Wang, C. Lithium-ion battery state of health monitoring and remaining useful life prediction based on support vector regression-particle filter. *J. Power Sources* **2014**, *271*, 114–123. [CrossRef]
5. Dong, G.; Chen, Z.; Wei, J.; Ling, Q. Battery health prognosis using Brownian motion modeling and particle filtering. *IEEE Trans. Ind. Electron.* **2018**, *65*, 8646–8655. [CrossRef]

6. Qiang, M.; Lei, X.; Cui, H.; Liang, W.; Pecht, M. Remaining useful life prediction of lithium-ion battery with unscented particle filter technique. *Microelectron. Reliab.* **2013**, *53*, 805–810.

7. Tang, S.; Yu, C.; Wang, X.; Guo, X.; Si, X. Remaining useful life prediction of lithium-ion batteries based on the wiener process with measurement error. *Energies* **2014**, *7*, 520–547. [CrossRef]

8. Long, B.; Xian, W.; Jiang, L.; Liu, Z. An improved autoregressive model by particle swarm optimization for prognostics of lithium-ion batteries. *Microelectron. Reliab.* **2013**, *53*, 821–831. [CrossRef]

9. Ahmadian, A.; Sedghi, M.; Elkamel, A.; Fowler, M.; Golkar, M.A. Plug-in electric vehicle batteries degradation modeling for smart grid studies: Review, assessment and conceptual framework. *Renew. Sustain. Energy Rev.* **2018**, *81*, 2609–2624. [CrossRef]

10. Gyan, P.; Aubret, P.; Hafsaoui, J. Experimental assessment of battery cycle life within the SIMSTOCK research program. *Oil Gas Sci. Technol. Rev. IFP Energ. Nouv.* **2013**, *68*, 137–147. [CrossRef]

11. Spotnitz, R. Simulation of capacity fade in lithium-ion batteries. *J. Power Sources* **2003**, *113*, 72–80. [CrossRef]

12. Laresgoiti, I.; Käbitz, S.; Ecker, M.; Sauer, D.U. Modeling mechanical degradation in lithium ion batteries during cycling: Solid electrolyte interphase fracture. *J. Power Sources* **2015**, *300*, 112–122. [CrossRef]

13. Purewal, J.; Wang, J.; Graetz, J.; Soukiazian, S.; Tataria, H.; Verbrugge, M.W. Degradation of lithium ion batteries employing graphite negatives and nickel–cobalt–manganese oxide plus spinel manganese oxide positives: Part 2, chemical–mechanical degradation model. *J. Power Sources* **2014**, *272*, 1154–1161. [CrossRef]

14. Jürgen, R.; Buchholz, M.; Meiler, M.; Bernreuter, P.; Dietmayer, K. State-of-health monitoring of lithium-ion batteries in electric vehicles by on-board internal resistance estimation. *J. Power Sources* **2011**, *196*, 5357–5363.

15. Weng, C.; Sun, J.; Peng, H. A unified open-circuit-voltage model of lithium-ion batteries for state-of-charge estimation and state-of-health monitoring. *J. Power Sources* **2014**, *258*, 228–237. [CrossRef]

16. Thompson, A.W. Economic implications of lithium ion battery degradation for vehicle-to-grid (v2x) services. *J. Power Sources* **2018**, *396*, 691–709. [CrossRef]

17. Wang, J.; Liu, P.; Hicks-Garner, J.; Sherman, E.; Soukiazian, S.; Verbrugge, M.; Tataria, H.; Musser, J.; Finamore, P. Cycle-life model for graphite-LiFePO4 cells. *J. Power Sources* **2011**, *196*, 3942–3948. [CrossRef]

18. Grolleau, S.; Delaille, A.; Gualous, H.; Gyan, P.; Revel, R.; Bernard, J.; Redondo-Iglesias, E.; Peter, J.; Network, S.I.M.C.A.L. Calendar aging of commercial graphite/LiFePO4 cell—Predicting capacity fade under time dependent storage conditions. *J. Power Sources* **2014**, *255*, 450–458. [CrossRef]

19. Liu, Y.; Xie, K.; Pan, Y.; Wang, H.; Li, Y.; Zheng, C. Simplified modeling and parameter estimation to predict calendar life of Li-ion batteries. *Solid State Ion.* **2018**, *320*, 126–131. [CrossRef]

20. Perez, A.; Quintero, V.; Jaramillo, F. Characterization of the degradation process of lithium-ion batteries when discharged at different current rates. *Proc. Inst. Mech. Eng. Part I J. Syst. Control Eng.* **2018**, *232*, 1075–1089. [CrossRef]

21. Cui, Y.; Du, C.; Yin, G.; Gao, Y.; Zhang, L.; Guan, T.; Yang, L.; Wang, F. Multi-stress factor model for cycle lifetime prediction of lithium ion batteries with shallow-depth discharge. *J. Power Sources* **2015**, *279*, 123–132. [CrossRef]

22. Su, L.; Zhang, J.; Wang, C.; Zhang, Y.; Li, Z.; Song, Y.; Jin, T.; Ma, Z. Identifying main factors of capacity fading in lithium ion cells using orthogonal design of experiments. *Appl. Energy* **2016**, *163*, 201–210. [CrossRef]

23. Su, L.; Zhang, J.; Huang, J.; Ge, H.; Li, Z.; Xie, F.; Liaw, B.Y. Path dependence of lithium ion cells aging under storage conditions. *J. Power Sources* **2016**, *315*, 35–46. [CrossRef]

24. Wang, J.; Purewal, J.; Liu, P.; Hicks-Garner, J.; Soukazian, S.; Sherman, E.; Sorenson, A.; Vu, L.; Tataria, H.; Verbrugge, M.W. Degradation of lithium ion batteries employing graphite negatives and nickel–cobalt–manganese oxide plus spinel manganese oxide positives: Part 1, aging mechanisms and life estimation. *J. Power Sources* **2014**, *269*, 937–948. [CrossRef]

25. Ecker, M.; Nieto, N.; Käbitz, S.; Schmalstieg, J.; Blanke, H.; Warnecke, A.; Sauer, D.U. Calendar and cycle life study of Li(NiMnCo)O2-based 18650 lithium-ion batteries. *J. Power Sources* **2014**, *248*, 839–851. [CrossRef]

26. Deshpande, R.; Verbrugge, M.; Cheng, Y.T.; Wang, J.; Liu, P. Battery cycle life prediction with coupled chemical degradation and fatigue mechanics. *J. Electrochem. Soc.* **2012**, *159*, A1730–A1738. [CrossRef]